

Single crystal growths and magnetic properties of hexagonal polar semimetals $RAuGe$ ($R = Y, Gd-Tm, \text{ and } Lu$)

Takashi Kurumaji,¹ Masaki Gen,^{1,2} Shunsuke Kitou,² Kazuhiko Ikeuchi,³ Mitsutaka Nakamura,⁴ Akihiko Ikeda,⁵ and Taka-hisa Arima^{1,2}

¹*Department of Advanced Materials Science, University of Tokyo, Kashiwa 277-8561, Japan*

²*RIKEN Center for Emergent Matter Science (CEMS), Wako 351-0198, Japan*

³*Neutron Science and Technology Center, Comprehensive Research Organization for Science and Society (CROSS), Tokai, Ibaraki, 319-1106, Japan*

⁴*J-PARC Center, Japan Atomic Energy Agency, Tokai, Ibaraki 319-1195, Japan*

⁵*Department of Engineering Science, University of Electro-Communications, Chofu, Tokyo 182-8585, Japan*

(Dated: January 10, 2023)

We study structural and magnetic properties of rare-earth based semimetals $RAuGe$ ($R = Y, Gd-Tm, \text{ and } Lu$) using flux-grown single crystals. These compounds belong to the noncentrosymmetric polar space group $P6_3mc$. We confirm the systematic structural evolution at room temperature as a function of ionic radius of rare earths to clarify the isopointal crossover between two polar structures: three-dimensional LiGaGe-type and quasi-two-dimensional NdPtSb-type. Magnetism shows a characteristic anisotropy in reasonable agreement with the crystal electric field (CEF) theory; the easy-plane-type anisotropy for $R = Tb$ and Dy turns into the Ising-type anisotropy for $R = Er$ and Tm . We evaluate the CEF parameters based on the Stevens operators to reasonably reproduce the temperature dependence of magnetic susceptibilities and specific heat for $RAuGe$ ($R = Tb-Tm$). The estimated energy scale of the Ising gap (~ 11 meV) in $TmAuGe$ is consistent with an excitation observed in an inelastic neutron scattering experiment. These findings suggest an opportunity for interplay between conduction electrons and nontrivial spin structures in the family of magnetic polar semimetals $RAuGe$.

INTRODUCTION

Polar metals are defined as the conductive materials with symmetry breaking allowing electric polarization, which provide a possible route to ferroelectric metals [1, 2] and to hyperferroelectricity [3, 4]. These materials are potentially applied to electric-field-switchable spintronic devices [5, 6], and a metallic counterpart of multiferroics [7–9] with topological band crossings induced by magnetic correlation [10, 11] and/or spin textures [12–15].

Rare-earth-based semimetals $RAuGe$ ($R = Sc, Y, La-Nd, Sm, Gd-Tm, \text{ and } Lu$) belong to the equiatomic ternary RTX ($T =$ transition metals, $X =$ p-block elements) intermetallic phases [16] of the hexagonal polar space group $P6_3mc$ (No. 186) [17, 18]. Their crystal structure is shown in Fig. 1(a), where the positions of Au and Ge are shifted upward and downward, respectively, along the c axis from the aristotype $ZrBeSi$ structure (space group $P6_3/mmc$, No. 194) to break the inversion symmetry, which is in common with a prototypical polar metal considered in theories [3, 7–11, 19–22].

CeAuGe and TmAuGe are known to show ferromagnetism below $T_C = 10$ K [23–25] and $T_C = 4$ K [26], respectively. The compounds for other R (Nd, and Gd–Er) are antiferromagnetic with a transition temperature T_N ranging between 6 K and 17 K [25, 27–32]. A previous neutron study detected a commensurate modulation vector $(\frac{1}{2}, 0, 0)$ in the ground state for $R = Tb-Er$ [27, 29–31]. Incommensurate modulations were also ob-

served to coexist at low temperatures or just below T_N , suggesting inherent magnetic frustration in triangular-lattice layers of R . The density of state has a pseudo-gap nature near the Fermi level due to the overlap of electron and hole bands, which is enabled by nominal valence configuration $R^{3+}Au^+Ge^{4-}$ [18, 33, 34] and contributes to semimetallic transport properties of nonmagnetic compounds ($R = Sc, Y, La, \text{ and } Lu$) [25, 33]. Resistivities of magnetic compounds, $RAuGe$ ($R = Ce, Nd, Gd, Ho, \text{ and } Tm$) [23, 26, 31, 32], are known to show nonmonotonic temperature dependences indicating a coupling with magnetic orders. These features suggest an opportunity to encounter unconventional properties of polar semimetals intertwined with frustrated magnetism in magnetic $RAuGe$. The above-mentioned physical properties were identified using polycrystals, and single crystal growths are only known for CeAuGe using Czochlarski and floating-zone methods [27, 35], and for epitaxial thin-film form of LaAuGe [36].

In this study, we report the single-crystal growths and physical properties of $RAuGe$ ($R = Y, Gd-Tm, \text{ and } Lu$). We analyzed the crystal structure using x-ray radiation to confirm the systematic evolution of polar structure as a function of R -ionic radius. We measured specific heat, magnetization, and thermal expansion to reveal the anisotropic magnetism significantly affected by the crystal electric field (CEF) as well as magnetic transitions at low temperatures. We estimate the CEF potential parameters to reproduce the magnetic susceptibility and specific heat and obtain a systematic R dependence reasonably agreed with the Stevens theory [37]. The esti-

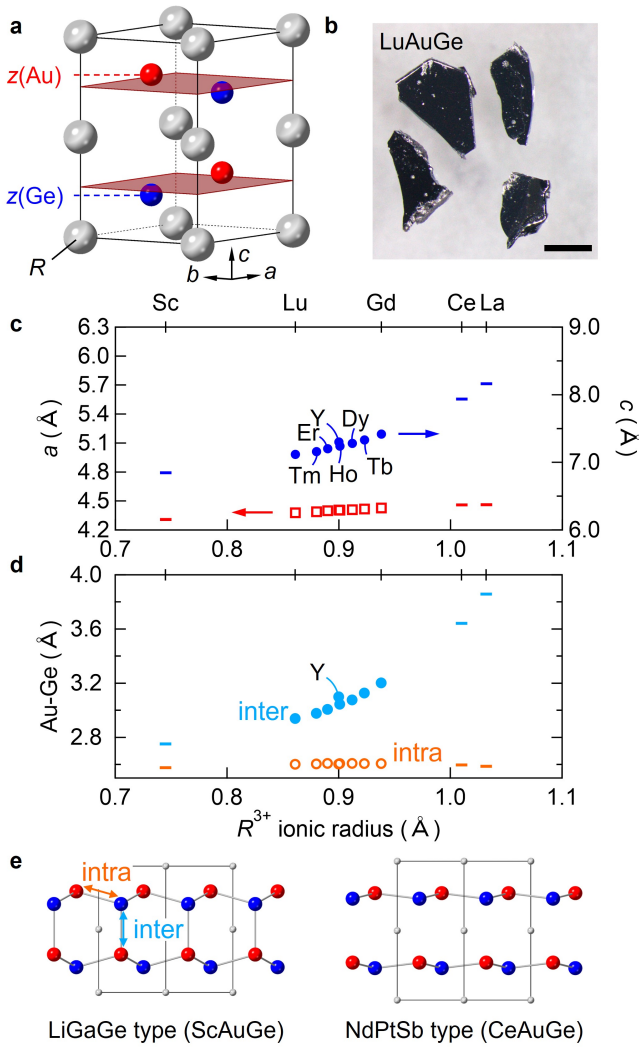


FIG. 1. (a) Crystal structure of $RAuGe$. $z(\text{Au})$ and $z(\text{Ge})$ are fractional coordinates along the c axis of Au and Ge atoms at $2b$ sites ($\frac{1}{3}, \frac{2}{3}, z$), which are shifted upward from 0.75 and downward from 0.25, respectively, producing the polarity in $RAuGe$. (b) Photograph of single crystals of $LuAuGe$. Black bar is 1 mm. (c)-(d) Lattice constants, a and c , and inter and intralayer Au-Ge bond lengths in a unit cell at room temperature as a function of the R^{3+} ionic radius for six-coordination. The values for $LaAuGe$ are excerpts from Ref. [33], and those for $CeAuGe$ and $ScAuGe$ are from Ref. [18]. (e) Side views of two isopointal [18] structures, LiGaGe and NdPtSb types, with distinct interlayer Au-Ge bonding (cyan arrow).

mated Ising gap in $TmAuGe$ is 11 meV, which is consistent with the excitation at 13 meV observed in the inelastic neutron scattering (INS) experiment. These results provide basic understanding on the structural and magnetic properties of the family of polar semimetals $RAuGe$.

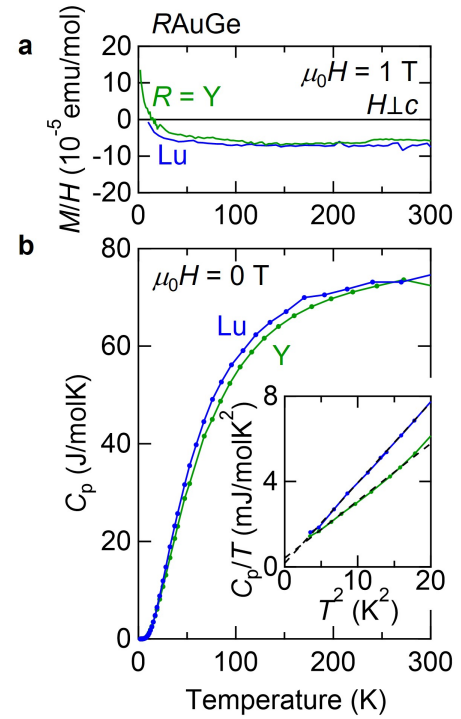


FIG. 2. (a)-(b) Temperature dependence of magnetic susceptibility (M/H) in $H \perp c$ and the specific heat (C_p) of $RAuGe$ ($R = Y$ and Lu) at zero field. The inset of (b) plots C_p/T vs. T^2 . The dashed lines are linear fit.

EXPERIMENTAL METHODS

Single crystals of $RAuGe$ ($R = Y, Gd-Tm$, and Lu) were grown using the Au-Ge self-flux method. The molar ratio of $R:Au:Ge$ was 1:2:2 for $R = Y, Tb-Tm$, and Lu and 1:3:3 for $R = Gd$. Starting materials were R ingot (99.9%), Au wire (99.5%), and Ge chunks (99.999%). They were loaded into an alumina crucible, which was sealed in an evacuated quartz tube. The tube was heated to 1100 °C and kept at this temperature for 24 hours before being slowly cooled to 800 °C in 200 hours. After being kept at 800 °C for 4 days, the tube was taken out from the furnace and centrifuged to remove excess flux. The obtained crystals were of platelet shape with typical dimensions $3 \times 3 \times 0.5$ mm³ as shown in Fig. 1(b). The atomic composition and the phase were checked by energy dispersive x-ray spectroscopy (EDS, JEOL model JSM-6010LA) and a powder x-ray diffraction (Rigaku SmartLab diffractometer) using $Cu K\alpha$ radiation, respectively. Single-crystal X-ray diffraction data for $RAuGe$ were collected on Rigaku AFC-8 diffractometer equipped with a HyPix-6000 detector using $Mo K\alpha$ radiation at room temperature. The intensities of Bragg reflections were collected by CrysAlisPro program [38]. The crystal structures were solved by SUPERFLIP [39] and refined by Jana2006 [40]. The details of the structural analy-

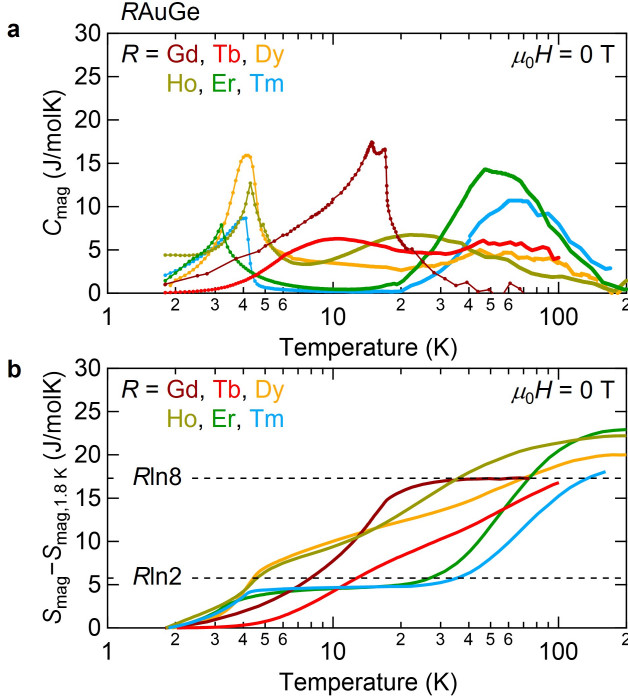


FIG. 3. (a)-(b) Temperature dependence of magnetic part of specific heat (C_{mag}) and that of entropy (S_{mag}) of $RAuGe$ ($R = \text{Gd-Tm}$) in zero field. $LuAuGe$ data was used to subtract the phonon background.

sis results are shown in supplementary materials. Attempts to grow the $P6_3mc$ phase for $YbAuGe$ [17] were unsuccessful and resulted in the orthorhombic phases, consistent with α -, β - (space group $Pnma$, No. 62) or γ - $YbAuGe$ (space group $Imma$, No. 74) as reported in Ref. [41].

Specific heat C_p was measured using a commercial system (heat capacity option of a Quantum Design PPMS). Magnetization was measured using a superconducting quantum interference device magnetometer (Quantum Design MPMS-XL). Thermal expansion was measured by the fiber-Bragg-grating (FBG) technique using an optical sensing instrument (Hyperion si155, LUNA) in a cryostat equipped with a superconducting magnet (Oxford Spectromag). Optical fibers were glued using epoxy (Stycast1266) on a (001) surface of as-grown crystals to measure the elongation or compression along the ab plane.

INS experiments were performed on a time-of-flight (TOF) spectrometer (4SEASONS) at the Materials and Life Science Experimental Facility (MLF) of J-PARC in Japan [42]. Polycrystalline $TmAuGe$ sample of 5 g was prepared by arc melting of elements. A boule of $TmAuGe$ was annealed at 500 °C for 21 days in an evacuated quartz tube, and sliced into pieces with thickness of 3 mm to reduce the absorption of neutrons. The chopper frequency was set to 200 Hz, and the incident energy of $E_i = 41$ meV was used to observe low-energy excitations. The

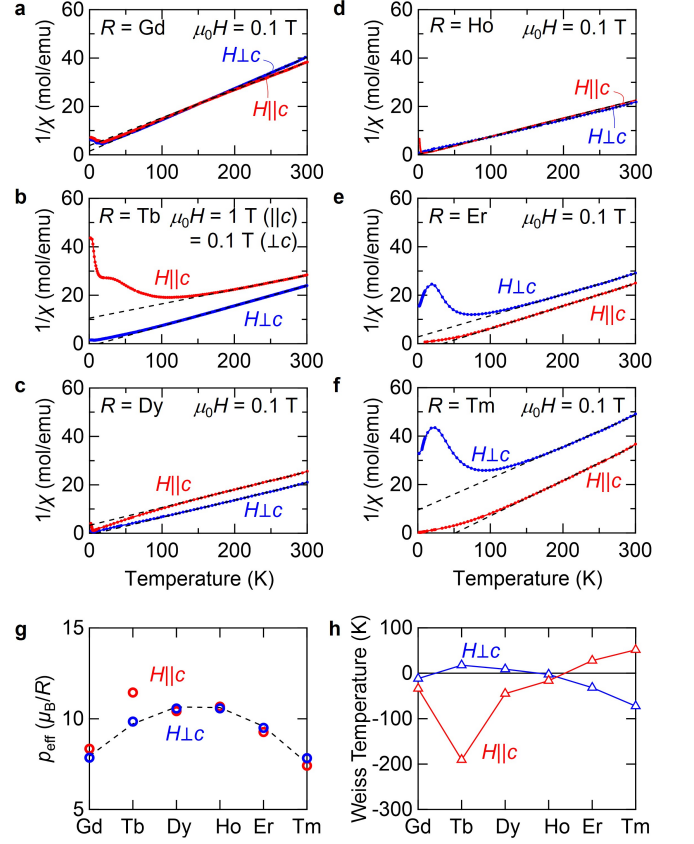


FIG. 4. (a)-(f) Temperature dependence of the inverse magnetic susceptibility (H/M) of $RAuGe$ ($R = \text{Gd-Tm}$) for $H \parallel c$ (red) and $H \perp c$ (blue). Dashed lines are Curie-Weiss fit to the data in $T = 150\text{-}300$ K. (g)-(h) R dependence of (g) effective magnetic moment (p_{eff}), and (h) Weiss temperature. Dashed line in (a) is free ions values.

sample was set in a GM refrigerator to control the temperature down to 5 K. The acquired data were analyzed with the UTSUSEMI software package [43].

RESULTS

The crystal structures of $RAuGe$ are systematically dependent on the ionic radius of R . Single-crystal x-ray diffraction confirms the polar $P6_3mc$ structure for all R , consistent with the previous reports [17, 18, 33]. Figures 1(c) and (d) display the R^{3+} ionic radius dependence of the lattice constants and inter- and intralayer Au-Ge bond lengths. Larger R ions lead to the expansion of the unit-cell volume especially resulting in the elongation of the c axis. This tendency correlates with the weakening of puckered distortion of Au-Ge honeycomb layer, where the out-of-plane (interlayer) Au-Ge bond becomes longer (see Fig. 1(d)). $ScAuGe$ has the smallest R radius ($Sc^{3+}(\text{VI}):0.745$ Å) with the interlayer Au-Ge bond of 275.2 pm, while it elongates to 385.8 pm in $LaAuGe$ with

the largest R -ion radius ($\text{La}^{3+}(\text{VI}):1.032 \text{ \AA}$) [44]. The materials for $R = \text{Y, Gd-Tm}$, and Lu smoothly interpolate the two extremes to verify the isopointal crossover of the crystal-structure type between NdPtSb type and LiGaGe type (Fig. 1(e)), both of which belong to the space group $P6_3mc$ [18, 23, 45]. In other words, as the ionic R^{3+} becomes larger, Au-Ge networks evolve from three-dimensional ZnO-type to staggered stacking of two-dimensional puckered binary honeycomb layers, asymptotically towards hBN-type network in the centrosymmetric ZrBeSi-type structure (space group $P6_3/mmc$, No. 194).

Next, we look through the physical properties of non-magnetic YAuGe and LuAuGe. Magnetic susceptibility (Fig. 2(a)) shows diamagnetic nature for both compounds at high temperatures, which is consistent with the previous report [33]. The low-temperature rise is ascribable to magnetic impurities. Specific heat C_p (Fig. 2(b)) is dominated by lattice contribution while C_p for LuAuGe is larger than that of YAuGe in the entire temperature range because of the lower Debye temperature [33]. Small electronic contribution, γT , to C_p is deduced by C_p/T -vs.- T^2 plot (see inset of Fig. 2(b)). Densities of states at Fermi energy per a formula unit for YAuGe and LuAuGe are 0.175 eV^{-1} ($\gamma = 0.4 \text{ mJ/mol K}^2$) and 0.085 eV^{-1} ($\gamma = 0.2 \text{ mJ/mol K}^2$), respectively, the order of magnitude of which agrees with the previous study [33].

Using C_p of LuAuGe as the reference for the lattice contribution, we obtain the magnetic specific heat (C_{mag}) for $R = \text{Gd-Tm}$ (Fig. 3(a)). The double peak structure at $T = 15$ and 17 K for $R = \text{Gd}$ reproduces the previous measurement [25]. The peaks below 10 K for $R = \text{Dy-Tm}$ represent magnetic transitions at low temperatures while a Schottky peak around $50\text{-}60 \text{ K}$ for $R = \text{Er}$ and Tm , for example, suggests the significant contribution of crystal electric field (CEF) excitations. To gain insight on the CEF energy level, we integrate C_{mag}/T with respect to T to estimate the magnetic entropy S_{mag} (Fig. 3(b)). For $R = \text{Gd}$, the most of S_{mag} for free-spin value, $R \ln 8$, is released below the transition temperatures owing to the Heisenberg nature of Gd spins. The release of S_{mag} between 4 and 20 K for ErAuGe and TmAuGe only approaches $R \ln 2$, suggesting the contribution of the lowest-lying (quasi-)doublet well isolated from excited states. This feature reflects on the Ising-type anisotropy of their magnetic moments. For $R = \text{Tb-Ho}$, in contrast, the T -dependence of S_{mag} does not show any saturation behavior below 100 K , suggesting overlapped contributions of CEF excitations.

The systematic R -dependence of magnetic anisotropy can be seen in the inverse magnetic susceptibility (H/M) summarized in Figs. 4(a)-(f). Magnetic properties for $R = \text{Gd}$ and Ho are roughly isotropic showing similar in- and out-of-plane M/H . For $R = \text{Tb}$ and Dy , easy-plane-type anisotropy is observed, while ErAuGe and TmAuGe host easy-axis-type anisotropy. All the compounds show

a Curie-Weiss behavior at high temperatures, where the Curie constants and the Weiss temperatures (Θ_W) are obtained by a linear fit of the H/M - T curve between 150 and 300 K . The effective moment p_{eff} is evaluated from the Curie constant. The R dependences of p_{eff} and Θ_W are summarized in Figs. 4(g) and (h). Except for $R = \text{Tb}$, p_{eff} agrees well with the free-ion value (dashed curve in Fig. 4(g)), suggesting that the energy scale of CEF is lower than the thermal energy at room temperature. Θ_W for $H \parallel c$ is larger than that for $H \perp c$ in the case of $R = \text{Er}$ and Tm . The systematic anisotropy change is associated with the CEF parameters [37].

We discuss the effect of CEF to clarify the R dependence of magnetic anisotropy in RAuGe. The 4f electrons on R sites in RAuGe are affected by the CEF potential (V_{CEF}) for the site symmetry of C_{3v} . V_{CEF} can be expressed by the Stevens operators (\hat{O}_n^m) as

$$V_{\text{CEF}} = B_{20}\hat{O}_2^0 + B_{40}\hat{O}_4^0 + B_{60}\hat{O}_6^0 + B_{43}\hat{O}_4^3 + B_{63}\hat{O}_6^3 + B_{66}\hat{O}_6^6. \quad (1)$$

Here, we assume $B_{43} = B_{63} = B_{66} = 0$ for simplicity of calculations, which is reasonable when the axial anisotropy of magnetic properties mainly arises from B_{20} , B_{40} , and B_{60} . In such a case the $|J_z = n\rangle$ state is also an eigenstate of V_{CEF} . In the high temperature limit, the $\hat{O}_2^0 = [3\hat{J}_z^2 - J(J+1)]$ term dominates the anisotropy of magnetic susceptibilities [46, 47]. The difference between the inverse of magnetic susceptibility for $H \parallel c$ and $H \perp c$, $\chi_{\parallel c}^{-1}$ and $\chi_{\perp c}^{-1}$, respectively, is approximated to be a constant as

$$\chi_{\parallel c}^{-1} - \chi_{\perp c}^{-1} = \frac{3(2J-1)(2J+3)}{2 \cdot 5C_{\text{ave}}} B_{20}, \quad (2)$$

where J is the total angular momentum $J = L \pm S$ and C_{ave} is the Curie constant obtained by their average for $H \parallel c$ and $H \perp c$. Assuming the identical radial distribution of 4f electron wave function for different R , B_{20} is predicted to be scaled with a Stevens factor α_J [37], which smoothly evolves from $R = \text{Tb}$ to Tm and changes the sign through Ho to Er . This feature of B_{20} agrees well with the R -dependence of magnetic susceptibility capturing the origin of the anisotropy switch in RAuGe, which will be discussed more quantitatively later.

To evaluate the systematic evolution of the CEF of R^{3+} ions, we simulate the temperature dependence of $\chi_{\parallel c}$, $\chi_{\perp c}$, and C_{mag} on the basis of the formulae (see e.g. Ref. [48]):

$$\chi_{\parallel c} = \frac{N_A(gJ\mu_B)^2}{Z} \times \frac{1}{k_B T} \sum_{n=-J}^J J_z^2 e^{-E_n/k_B T}, \quad (3)$$

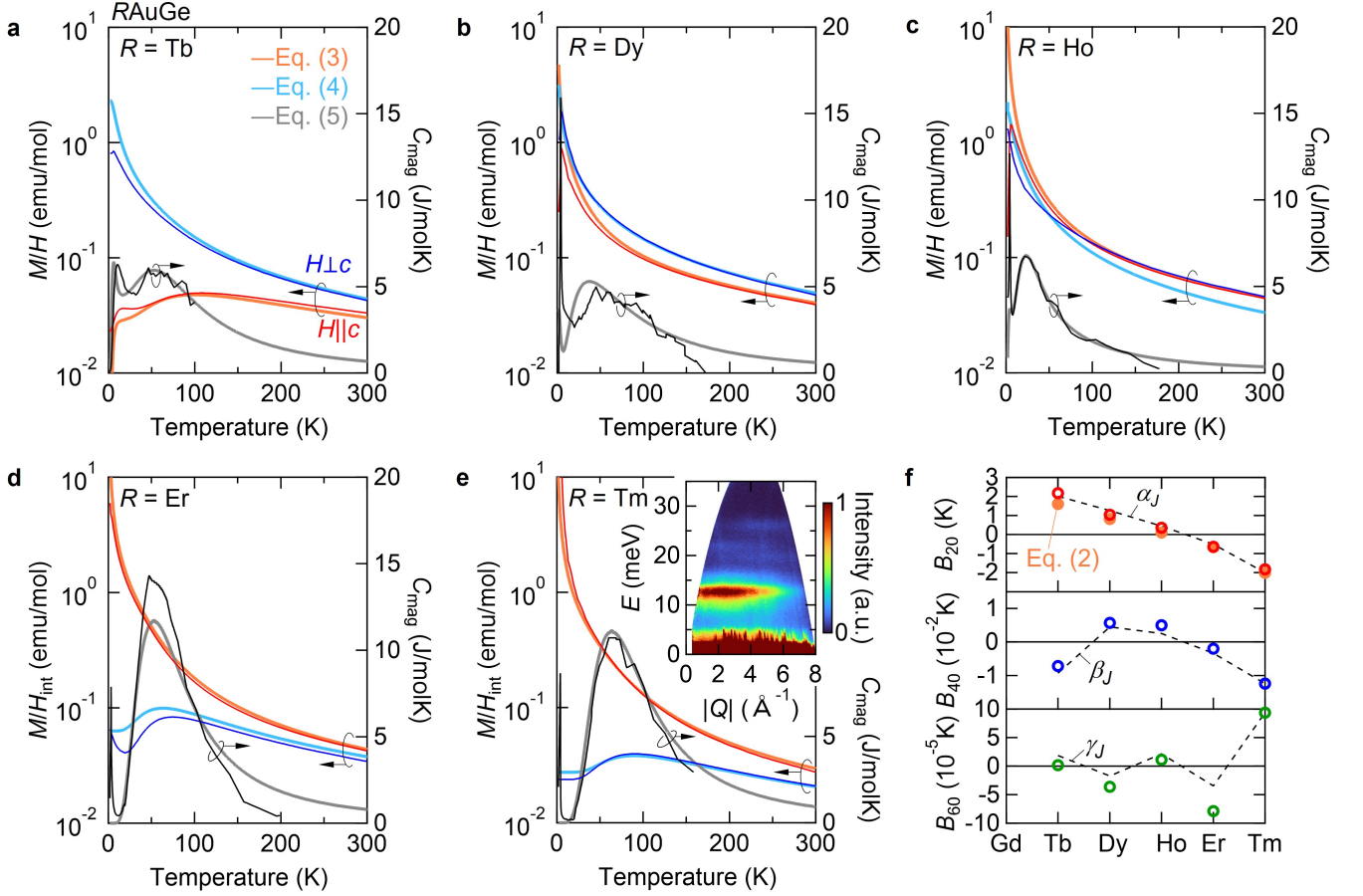


FIG. 5. (a)-(e) Temperature dependence of M/H for $H \parallel c$ (red) and $H \perp c$ (blue), and C_{mag} (black) of $RAuGe$ ($R = \text{Tb-Tm}$). Magnetic susceptibility of $ErAuGe$ and $TmAuGe$ for $H \parallel c$ (red curves in (d) and (e)) is corrected by the demagnetization factor, N_d , where M is divided by the internal magnetic field, $H_{\text{int}} (= H - N_d M)$. Cyan, orange, and gray curves are obtained from Eqs. (3)-(5), respectively (see text) with optimized parameters, B_{20} , B_{40} , and B_{60} (see supplementary materials). Inset of (e) is a color map of intensity vs. $|Q|$ of the polycrystalline INS profile of $TmAuGe$ with the incident neutron energy $E_i = 41$ meV at $T = 5$ K. (f) R dependence of B_{20} , B_{40} , and B_{60} (open circles). Dashed lines are Stevens factors, α_J , β_J , and γ_J [37], normalized by the values for $R = \text{Tm}$. Closed orange circles in (f) is obtained from the anisotropy of Curie-Weiss curves using Eq. (2).

$$\chi_{\perp c} = \frac{2N_A(gJ\mu_B)^2}{Z} \times \sum_{n=-J}^{J-1} |\langle n+1 | J_x | n \rangle|^2 \frac{e^{-E_n/k_B T} - e^{-E_{n+1}/k_B T}}{E_{n+1} - E_n}, \quad (4)$$

$$C_{\text{mag}} = \frac{N_A}{k_B T^2} \left[\left(\frac{1}{Z} \sum_n E_n^2 e^{-E_n/k_B T} \right) - \left(\frac{1}{Z} \sum_n E_n e^{-E_n/k_B T} \right)^2 \right], \quad (5)$$

where N_A is Avogadro constant, k_B is Boltzmann constant, μ_B is Bohr magneton, gJ is Lande's g factor, E_n is the energy for a state, $|J_z = n\rangle$. $Z = \sum_n e^{-E_n/k_B T}$ is the partition function. We summarize the results of simulation of magnetic susceptibilities and magnetic specific heat in Figs. 5(a)-(e), and the deduced Stevens parameters in Fig. 5(f). We note that all the Stevens parameters systematically scale with the Stevens factors, α_J , β_J , and γ_J , confirming the validity of the simulations. We also show the B_{20} values estimated from the formula of high- T limit Eq. (2) (closed orange circle) in Fig. 5(f), agreeing well with the all-data analysis.

To double check the CEF gap in $TmAuGe$, we perform INS and observe the energy transfer as shown in the inset of Fig. 5(e). Crystal field around a Tm^{3+} ion in C_{3v} symmetry splits the $J = 6$ manifold of Tm^{3+} $4f^{12}$ levels into five singlets and four doublets. The lowest quasi-

TABLE I. Structural and magnetic parameters of $RAuGe$ ($R = Y, Gd-Tm, \text{ and } Lu$). a, c : lattice constants, and z_{Au}, z_{Ge} : fractional coordinate for Au and Ge atoms along the c axis (see supplementary materials). T_C : ferromagnetic transition temperature. T_N : antiferromagnetic transition temperature. p_{eff} : effective magnetic moment, and Θ_W : Weiss temperature for $H \parallel c$ and $H \perp c$.

R	Y	Gd	Tb	Dy	Ho	Er	Tm	Lu
Structural parameters								
a (Å)	4.4061(2)	4.42799(1)	4.4177(2)	4.4105(3)	4.4045(2)	4.3996(2)	4.3879(3)	4.3772(3)
c (Å)	7.3011(4)	7.4176(2)	7.3300(3)	7.2801(4)	7.2402(4)	7.2018(3)	7.1594(5)	7.1175(3)
z_{Au}	0.78435(5)	0.77968(6)	0.78308(7)	0.78614(11)	0.78703(6)	0.78931(6)	0.79083(7)	0.79415(9)
z_{Ge}	0.2088(2)	0.2114(3)	0.2097(3)	0.2088(6)	0.2075(3)	0.2069(3)	0.2068(3)	0.2071(5)
Magnetic properties								
T_C (K)	-	-	-	-	-	-	4.1	-
T_N (K)	-	17.0	6.0	4.4	4.9	3.2	-	-
$p_{eff \perp c}$	-	7.9	9.8	10.6	10.6	9.5	7.8	-
$\Theta_{W \perp c}$ (K)	-	-11.6	17.6	9.0	-2.6	-31.8	-72.3	-
$p_{eff \parallel c}$	-	8.3	11.4	10.4	10.7	9.5	7.4	-
$\Theta_{W \parallel c}$ (K)	-	-33.8	-191	-45.0	-16.6	33.0	51.6	-

doublet is mainly composed of $J_z = \pm 6$, and the CEF splitting between the quasi-doublet and $J_z = \pm 5$ doublet provides Ising nature of the magnetic moment. At 5 K, dispersionless excitations are observed at around 13 meV, which is consistent with the calculation on the basis of Eqs. (3)-(5) giving the energy splitting of 11 meV (see supplementary materials). We note that the lowest quasi-doublet should have a tiny gap due to the non-Kramers nature of a $Tm^{3+}(4f^{12})$ ion [49, 50], if one considers the effect of CEF potentials $\hat{O}_n^{\pm 3}$ ($n = 4, 6$) in Eq. (1), which has remained unresolved in the present study.

Established the magnetic anisotropy originating from the CEF in $RAuGe$, we focus on the magnetic transitions at low temperatures. Figures 6(a)-(l) show the susceptibility at $\mu_0 H = 0.1$ T as well as specific heat and thermal expansion at zero field near the transition temperatures. Together with the structural parameters, we summarize the magnetic properties in Table I.

Figures 6(a) and (b) compare the temperature dependences of physical properties of $GdAuGe$. All the measurements were performed by using a unique single crystal. There are anomalies in M/H for both $H \parallel c$ and $H \perp c$ (Fig. 6(a)) indicating two successive magnetic transitions at $T_N = 16.9$ K and $T_{mag} = 10.0$ K. In the specific heat measurement (Fig. 6(b)), on the other hand, we observed two anomalies at $T_N = 17.0$ K and $T_{HC} = 14.8$ K, reproducing the previous study [25]. Note that the observed lattice-length change below T_N can be mainly attributed to the exchange striction because the CEF anisotropy is absent [51]. No obvious anomaly at T_{mag} or T_{HC} potentially suggests that these transitions are related with spin-orientation change keeping $\mathbf{S}_i \cdot \mathbf{S}_j$ for local Gd spin moments (\mathbf{S}_i) unchanged. Aside from the clear antiferromagnetic transition at 17 K, we observed secondary anomalies at different temperatures, T_{mag} and T_{HC} , through different probes because each anomaly is too subtle to be seen through the other properties. It

is a possible future study to develop the magnetic phase diagram and to identify the evolution of the magnetic structures at low temperatures.

The magnetic phase transition of $TbAuGe$ takes place at $T_N = 6$ K as seen as a peak of M/H for $H \perp c$ (Fig. 6(c)) and a tiny shoulder-type anomaly in C_{mag} (Fig. 6(d)). For $H \parallel c$, M/H shows a kink at T_N and is well suppressed in contrast to that for $H \perp c$ owing to the strong easy-plane type anisotropy. Thermal expansion shows an anomaly at T_N . We note that the lowest CEF level for the non-Kramers Tb^{3+} ion is a non-magnetic singlet isolated from the lowest excited state. The energy scale of the separation is estimated to be 15 K on the basis of the simulation (see supplementary materials). Magnetic ordering in such a singlet-ground-state system is enabled by induced-moment instability upon the exchange interaction exceeding the CEF gap [52, 53]. This is consistent with the suppressed C_{mag} peak at T_N as observed in Pr-based compounds [54–56]. An additional anomaly associated with an incommensurate-commensurate transition is not identified down to $T = 1.8$ K in our measurements. A diffraction study is to be reported in future.

The antiferromagnetic transition in $DyAuGe$ is clearer than that in $TbAuGe$ as shown as a drop of M/H at $T_N = 4$ K (Fig. 6(e)). For $H \perp c$, the $M-T$ curve shows a hysteresis at lower temperatures, suggesting that the in-plane magnetic field induces rearrangement of the magnetic domains breaking C_6 symmetry of the crystal. This is consistent with a hysteresis also seen in the in-plane thermal expansion (Fig. 6(f)). The M/H shows a drop below T_N for both $H \parallel c$ and $H \perp c$, suggesting that the magnetic moments can have both in- and out-of-plane components. The temperature derivative dM/dT for $H \perp c$ shows a peak clarifying T_N (see the orange arrow in Fig. 6(e)). The magnetic transition appears as a broad peak of specific heat (Fig. 6(f)) while the successive nature is not clearly resolved.

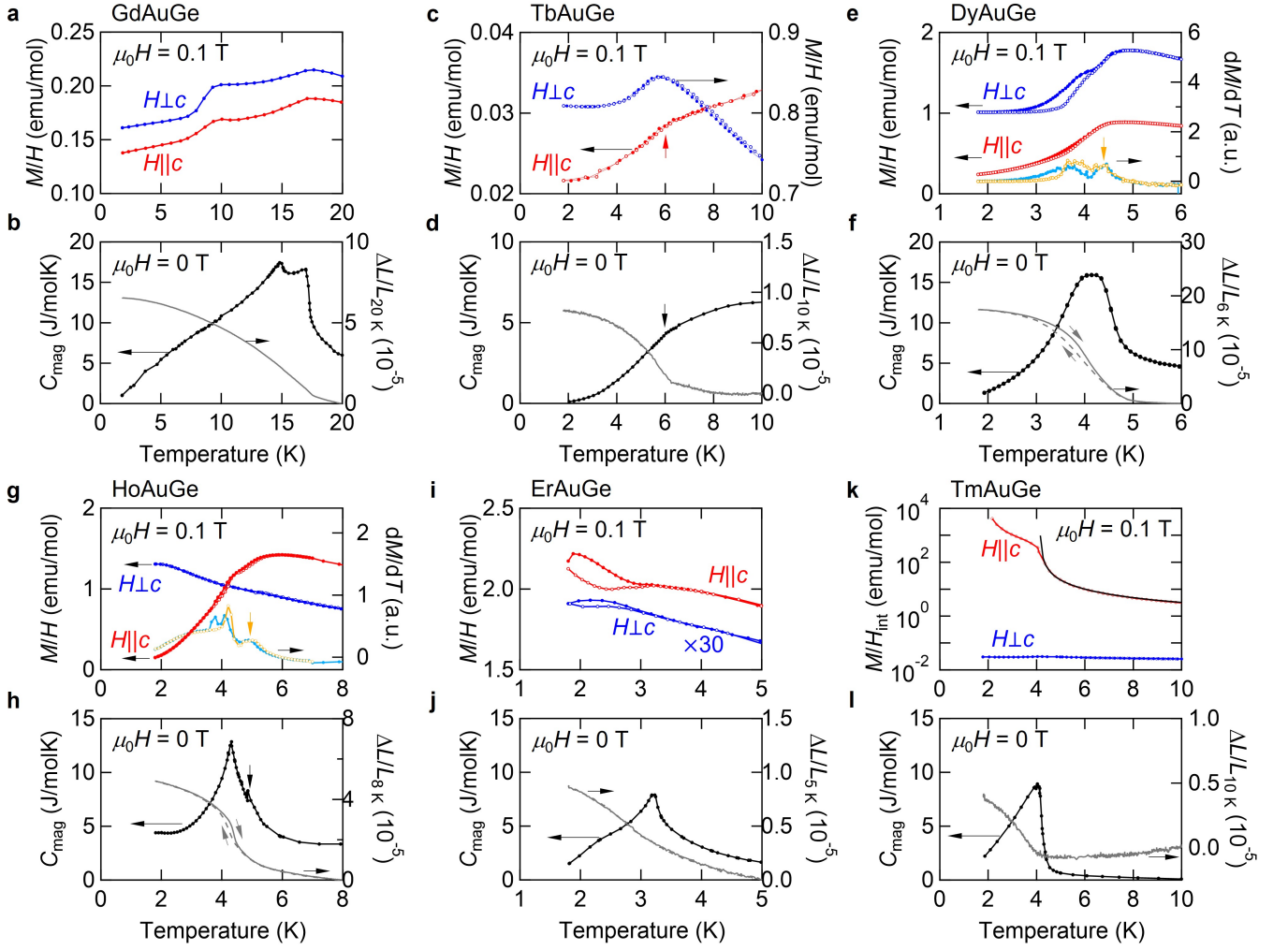


FIG. 6. (a)-(l) Temperature dependence of magnetic and thermodynamic properties of $RAuGe$ ($R = \text{Gd-Tm}$) at low temperatures. Red and blue curves represent M/H for $H \parallel c$ and $H \perp c$ at $\mu_0 H = 0.1$ T, respectively. Black and gray curves represent C_{mag} and in-plane $\Delta L/L_0$ in zero field. In (e) and (g), temperature derivative of M (dM/dT) for $H \perp c$ and $H \parallel c$, respectively, are shown. Closed (open) symbols and solid (dashed) lines are measured in temperature-decrease (increase) processes. In (k), demagnetization field is corrected by using the internal magnetic field, $H_{\text{int}} = H_{\text{ext}} - N_d M$. Black curve in (k) is the Curie-Weiss fit ($\chi_{\parallel c} = \frac{C_{\text{low}}}{T - \theta_{\parallel c, \text{low}}}$) for $4 \text{ K} < T < 30 \text{ K}$.

The magnetic susceptibility of HoAuGe is isotropic (with a subtle easy-plane nature) at high temperatures while an easy-axis nature is enhanced at low temperatures (Fig. 6(g)). The antiferromagnetic transition can be seen as a weak drop of M/H at $T_{N1} = 5$ K and a tiny peak in C_{mag} (black arrow in Fig. 6(h)). The main peak in the specific heat is observed at $T_{N2} = 4$ K, which is accompanied by a thermal-expansion jump and a kink in M/H for $H \parallel c$. The latter is more clearly seen in dM/dT (orange arrow in Fig. 6(g)). These anomalies are not discernible in M/H for $H \perp c$, potentially indicating the predominant c -axis component of the spin moment in the magnetic ordered states. The successive transitions support the previous neutron diffraction study, where a mixture of commensurate and incommensurate

orders was identified below $T_{N1} = 6$ K, which eventually developed to the pure commensurate order [29–31]. We do not observe multi-step anomalies at 5.6, 4, or 2 K in the specific heat measurement in contrast to a previous study [31] potentially because of the difference in sample quality or annealing condition.

ErAuGe shows an antiferromagnetic transition at $T_N = 3.2$ K. M - T curves (Fig. 6(i)) are hysteretic for both $H \parallel c$ and $H \perp c$ at low temperatures, suggesting a glassy nature of the magnetic order. Large easy-axis type anisotropy indicates that the magnetic moments are aligned along the c axis. The transition can be clearly identified as a specific-heat peak and a thermal-expansion kink (Fig. 6(j)). This is in contrast to the successive transitions at 3.7 K and 2.8 K associated with

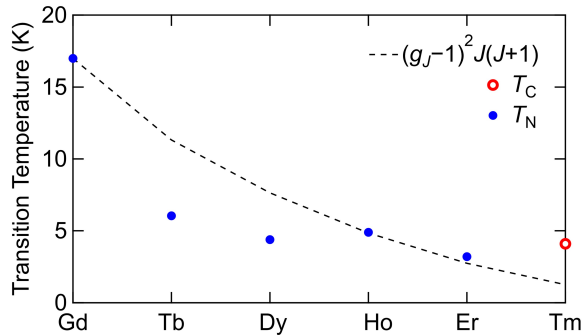


FIG. 7. R dependence of the transition temperatures. Blue (red) markers represent antiferromagnetic (ferromagnetic) transitions. Dashed line is the de Gennes factor $(g_J - 1)^2 J(J + 1)$ normalized by the Gd value.

the incommensurate-commensurate transition observed in previous neutron diffraction [29, 30].

TmAuGe is the only ferromagnetic system among $RAuGe$ for $R = Gd-Tm$, as identified in Ref. [26]. To see the divergence of magnetic susceptibility, we correct the demagnetization field for $H \parallel c$ (red curve in Fig. 6(k)). Corrected magnetic susceptibility is obtained by M/H_{int} . We fit the M/H_{int} curve for $H \parallel c$ at low temperatures to the Curie-Weiss law ($\chi_{\parallel c} = \frac{C_{\text{low}}}{T - \Theta_{\parallel c, \text{low}}}$) as shown by the black curve in Fig. 6(k). The Weiss temperature is $\Theta_{\parallel c, \text{low}} = 4.1$ K, consistent with T_C . We obtain the effective moment $p_{\text{Ising}} = 7.07\mu_B$ by the formula for the Curie constant $C_{\text{low}} = N_A p_{\text{Ising}}^2 / k_B$ in the case of the Ising-type magnetic moments. The obtained p_{Ising} agrees well with the expected value $p_{\text{Ising}} = g_J J = 7\mu_B$ for the lowest quasi-doublet composed of $J_z = \pm 6$ well separated from the lowest excited state, which is consistent with the CEF analysis.

Finally, we discuss the R dependence of magnetic transition temperature summarized in Fig. 7. On the basis of the de Gennes scaling rule [57], the transition temperatures among isostructural R compounds are supposed to be scaled with the de Gennes factor, $(g_J - 1)^2 J(J + 1)$ (see the dashed curve in Fig. 7). This argument is valid as long as the CEF effect and anisotropy of exchange interaction are negligible and Heisenberg-type RKKY interaction ($\mathcal{J}_{\text{ex}}(\mathbf{q}_{\text{mag}})$) stabilizes a magnetic order with the identical magnetic modulation vector \mathbf{q}_{mag} among $RAuGe$. We observe the breakdown of the de Gennes scaling as it overestimates T_N for Tb and Dy and underestimates T_C for Tm. Indeed, one of the above conditions is violated as the Tm compound is ferromagnetic ($\mathbf{q}_{\text{mag}} = (0, 0, 0)$) in contrast that the antiferromagnetic order with $\mathbf{q}_{\text{mag}} \sim (0.4-0.5, 0, 0)$ in the reciprocal lattice unit is favored for the other compounds [27, 29, 30]. We

have to consider the modification of $\mathcal{J}_{\text{ex}}(\mathbf{q}_{\text{mag}})$, which is potentially sensitive to subtle details of the band structure in the present semimetallic materials. We also note that the suppression of T_N for $R = Tb$ is reasonable because of the singlet ground state [58] while that of $R = Dy$ is nontrivial. Theories predict that the CEF effect is basically supposed to enhance the transition temperature in the case of the easy-axis type anisotropy ($B_{20} < 0$, not valid for $R = Dy$) [59, 60], but the suppression of T_N is possible when the easy-plane type anisotropy ($B_{20} > 0$) surpasses the exchange interaction [61]. The observed thermal expansion ($\Delta L/L \sim 1.7 \times 10^{-4}$) in DyAuGe is the largest in the present $RAuGe$ family, which may reflect the magnetoelastic strain originating from the magnetic anisotropy rather than the exchange striction. We might also have to consider the effect of magnetic frustration in DyAuGe to potentially promote the competition among noncollinear/noncoplanar magnetic structures suppressing T_N .

In summary, we succeeded in growing single crystals of $RAuGe$ for $R = Y, Gd-Tm$, and Lu and revealed the thermodynamic and magnetic properties. Magnetic anisotropy is systematically determined by the CEF effect of R ions, and low-temperature transitions are dominated by the lowest CEF levels. Continuous structural evolution of the polarity and its potential interplay with nontrivial magnetism would be viewed as a promising platform for studying metallic multiferroics [62, 63]. Findings in the present study provide basic understanding of single crystalline properties of a family of polar semimetal $RAuGe$. Transport properties intertwined with frustrated magnetism is a desired future study, which will be reported elsewhere.

T.K. was financially supported by Ministry of Education Culture Sports Science and Technology (MEXT) Leading Initiative for Excellent Young Researchers (JPMXS0320200135), Japan Society for the Promotion of Science (JSPS) KAKENHI Grant-in-Aid for Young Scientists B (No. 21K13874). M.G. was supported by the JSPS KAKENHI Grant-in-Aid for Scientific Research (No. 20J10988). S.K. was supported by JSPS KAKENHI Grant-in-Aid for Early-Career Scientists (No. 22K14010). This work was partly supported by JSPS KAKENHI Grant-in-Aid for Scientific Research on Innovative Areas Quantum Liquid Crystals (No. JP19H05826 and No. 19H01835). The neutron experiment at the Materials and Life Science Experimental Facility of the J-PARC was performed under a user program (Proposal No. 2022A0045). This work was partly performed using the facilities of the Materials Design and Characterization Laboratory in the Institute for Solid State Physics, the University of Tokyo. S.K. thanks K. Adachi and D. Hashizume for the support of the in-house XRD experiments.

-
- [1] Y. Shi, Y. Guo, X. Wang, A. J. Princep, D. Khalyavin, P. Manuel, Y. Michiue, A. Sato, K. Tsuda, S. Yu, *et al.*, “A ferroelectric-like structural transition in a metal,” *Nat. Mater.* **12**, 1024–1027 (2013).
- [2] N. A. Benedek and T. Birol, “Ferroelectric’ metals re-examined: fundamental mechanisms and design considerations for new materials,” *J. Mater. Chem. C* **4**, 4000 (2016).
- [3] K. F. Garrity, K. M. Rabe, and D. Vanderbilt, “Hyperferroelectrics: proper ferroelectrics with persistent polarization,” *Phys. Rev. Lett.* **112**, 127601 (2014).
- [4] W. X. Zhou and A. Ariando, “Review on ferroelectric/polar metals,” *Jpn. J. Appl. Phys.* **59**, SI0802 (2020).
- [5] A. Narayan, “Class of Rashba ferroelectrics in hexagonal semiconductors,” *Phys. Rev. B* **92**, 220101 (2015).
- [6] Z. Fei, W. Zhao, T. A. Palomaki, B. Sun, M. K. Miller, Z. Zhao, J. Yan, X. Xu, and D. H. Cobden, “Ferroelectric switching of a two-dimensional metal,” *Nature* **560**, 336–339 (2018).
- [7] W. Cao, P. Tang, Y. Xu, J. Wu, B.-L. Gu, and W. Duan, “Dirac semimetal phase in hexagonal LiZnBi,” *Phys. Rev. B* **96**, 115203 (2017).
- [8] H. Gao, Y. Kim, J. W. F. Venderbos, C. L. Kane, E. J. Mele, A. M. Rappe, and W. Ren, “Dirac-Weyl semimetal: Coexistence of Dirac and Weyl fermions in polar hexagonal ABC crystals,” *Phys. Rev. Lett.* **121**, 106404 (2018).
- [9] H. Gao, J. Strockoz, M. Frakulla, J. W. F. Venderbos, and H. Weng, “Noncentrosymmetric topological Dirac semimetals in three dimensions,” *Phys. Rev. B* **103**, 205151 (2021).
- [10] Y. Du, B. Wan, D. Wang, L. Sheng, C.-G. Duan, and X. Wan, “Dirac and weyl semimetal in $XYBi$ ($X = Ba, Eu$; $Y = Cu, Ag$ and Au),” *Sci. Rep.* **5**, 1–8 (2015).
- [11] C. Mondal, C. K. Barman, A. Alam, and B. Pathak, “Broken symmetry driven phase transitions from a topological semimetal to a gapped topological phase in $SrAgAs$,” *Phys. Rev. B* **99**, 205112 (2019).
- [12] J. Gaudet, H.-Y. Yang, S. Baidya, B. Lu, G. Xu, Y. Zhao, J. A. Rodriguez-Rivera, C. M. Hoffmann, D. E. Graf, D. H. Torchinsky, *et al.*, “Weyl-mediated helical magnetism in $NdAlSi$,” *Nat. Mater.* **20**, 1650–1656 (2021).
- [13] A. K. Srivastava, P. Devi, A. K. Sharma, T. Ma, H. Deniz, H. L. Meyerheim, C. Felser, and S. S. P. Parkin, “Observation of robust Néel skyrmions in metallic $PtMnGa$,” *Adv. Mater.* **32**, 1904327 (2020).
- [14] H. Zhang, D. Raftrey, Y.-T. Chan, Y.-T. Shao, R. Chen, X. Chen, X. Huang, J. T. Reichenadter, K. Dong, S. Susarla, *et al.*, “Room-temperature skyrmion lattice in a layered magnet $(Fe_{0.5}Co_{0.5})_5GeTe_2$,” *Sci. Adv.* **8**, eabm7103 (2022).
- [15] H. Zhang, Y.-T. Shao, R. Chen, X. Chen, S. Susarla, D. Raftrey, J. T. Reichenadter, L. Caretta, X. Huang, N. S. Settineri, *et al.*, “A room temperature polar magnetic metal,” *Phys. Rev. Mater.* **6**, 044403 (2022).
- [16] S. Gupta and K. G. Suresh, “Review on magnetic and related properties of RTX compounds,” *J. Alloys Compd.* **618**, 562 (2015).
- [17] D. Rossi, R. Marazza, and R. Ferro, “Ternary rare earth alloys: $RAuGe$ compounds,” *J. Alloys Compd.* **187**, 267 (1992).
- [18] R. Pöttgen, H. Borrmann, C. Felser, O. Jepsen, R. Henn, R. K. Kremer, and A. Simon, “Crystal and electronic structures of $ScAuGe$, $CeAuGe$, and $LuAuGe$: a transition from two- to three-dimensional $[AuGe]$ polyanions,” *J. Alloys Compd.* **235**, 170 (1996).
- [19] J. W. Bennett, K. F. Garrity, K. M. Rabe, and D. Vanderbilt, “Hexagonal ABC semiconductors as ferroelectrics,” *Phys. Rev. Lett.* **109**, 167602 (2012).
- [20] Q. D. Gibson, L. M. Schoop, L. Muechler, L. S. Xie, M. Hirschberger, N. P. Ong, R. Car, and R. J. Cava, “Three-dimensional Dirac semimetals: design principles and predictions of new materials,” *Phys. Rev. B* **91**, 205128 (2015).
- [21] D. Di Sante, P. Barone, A. Stroppa, K. F. Garrity, D. Vanderbilt, and S. Picozzi, “Intertwined Rashba, Dirac, and Weyl fermions in hexagonal hyperferroelectrics,” *Phys. Rev. Lett.* **117**, 076401 (2016).
- [22] H. Zhang, W. Huang, J.-W. Mei, and X.-Q. Shi, “Influences of spin-orbit coupling on Fermi surfaces and Dirac cones in ferroelectriclike polar metals,” *Phys. Rev. B* **99**, 195154 (2019).
- [23] R. Pöttgen, H. Borrmann, and R. K. Kremer, “Ferro-magnetic ordering in $CeAuGe$,” *J. Magn. Magn. Mater.* **152**, 196 (1996).
- [24] B. J. Gibson, R. Pöttgen, and R. K. Kremer, “Magnetic structure determination of $CeAuGe$ and $CeAgGe$,” *Physica B: Condensed Matter* **276**, 734 (2000).
- [25] B. J. Gibson, W. Schnelle, R. Pöttgen, K. Bartkowski, and R. K. Kremer, “Susceptibility, specific heat, and transport properties of $CeAuGe$ and $GdAuGe$,” *Czechoslovak Journal of Physics* **46**, 2573 (1996).
- [26] D. Kaczorowski and A. Szytuła, “Magnetic, thermal and electrical transport properties of $TmAuGe$,” *J. Alloys Compd.* **614**, 186 (2014).
- [27] B. J. Gibson, *Investigation of the physical properties of the ternary intermetallic rare-earth compounds, $RETGe$ ($RE = Sc, Y, La-Lu$; $T = Ag, Au$)*, Ph.D. thesis, Loughborough University (1998).
- [28] B. Penc, S. Baran, M. Ślaski, and A. Szytuła, “Magnetic properties of $RAuGe$ compounds ($R = Pr, Nd, Tb-Er$),” *J. Alloys Compd.* **282**, L6 (1999).
- [29] S. Baran, M. Hofmann, B. Penc, M. Ślaski, A. Szytuła, and A. Zygmunt, “Magnetic structures of $RAuGe$ ($R = Pr, Nd, Tb, Ho, Er$) compounds,” *Physica B* **276**, 656 (2000).
- [30] S. Baran, M. Hofmann, G. Lampert, N. Stüsser, A. Szytuła, D. Többens, P. Smeibidl, and S. Kausche, “Neutron diffraction studies of the magnetic structures of $HoAuGe$ and $ErAuGe$,” *J. Magn. Magn. Mater.* **236**, 293 (2001).
- [31] B. J. Gibson, R. Pöttgen, W. Schnelle, B. Ouladdiaf, and R. K. Kremer, “Crystal and magnetic structure of antiferromagnetic $HoAuGe$,” *J. Phys.: Condens. Matter* **13**, 2593 (2001).
- [32] A. K. H. Bashir, M. B. Tchoula Tchokonté, J. L. Snyman, B. M. Sondezi, and A. M. Strydom, “Antiferromagnetic ordering in $NdAuGe$ compound,” *J. Appl. Phys.* **115**, 17E134 (2014).
- [33] W. Schnelle, R. Pöttgen, R. K. Kremer, E. Gmelin, and O. Jepsen, “The crystal structure, magnetic susceptibility, electrical resistivity, specific heat, and electronic band structure of $RAuGe$ ($R = Sc, Y, La, Lu$),” *J. Phys.: Condens. Matter* **9**, 1435 (1997).

- [34] Y. Wang, K. G. Koster, A. M. Ochs, M. R. Scudder, J. P. Heremans, W. Windl, and J. E. Goldberger, “The chemical design principles for axis-dependent conduction polarity,” *J. Am. Chem. Soc.* **142**, 2812–2822 (2020).
- [35] A. Prokofiev and S. Paschen, “Crystal growth and stoichiometry of strongly correlated intermetallic cerium compounds,” in *Modern Aspects of Bulk Crystal and Thin Film Preparation* (IntechOpen, 2012).
- [36] D. Du, A. Lim, C. Zhang, P. J. Strohbeen, E. H. Shourov, F. Rodolakis, J. L. McChesney, P. Voyles, D. C. Fredrickson, and J. K. Kawasaki, “High electrical conductivity in the epitaxial polar metals LaAuGe and LaPtSb,” *APL Materials* **7**, 121107 (2019).
- [37] K. W. H. Stevens, “Matrix elements and operator equivalents connected with the magnetic properties of rare earth ions,” *Proc. Phys. Soc. Sect. A* **65**, 209 (1952).
- [38] Oxford Diffraction CrysAlisPRO, “Agilent Technologies UK Ltd,” Yarnton, England **1** (2014).
- [39] L. Palatinus and G. Chapuis, “SUPERFLIP—a computer program for the solution of crystal structures by charge flipping in arbitrary dimensions,” *J. Appl. Cryst.* **40**, 786–790 (2007).
- [40] Václav Petříček, Michal Dušek, and Lukáš Palatinus, “Crystallographic computing system JANA2006: general features,” *Z. Kristallogr. Cryst. Mater.* **229**, 345–352 (2014).
- [41] F. Merlo, M. Pani, F. Canepa, and M. L. Fornasini, “Phases around the 1:1:1 composition in the Yb-Au-Ge and Ca-Au-Ge systems,” *J. Alloys Compd.* **264**, 82–88 (1998).
- [42] R. Kajimoto, M. Nakamura, Y. Inamura, F. Mizuno, K. Nakajima, S. Ohira-Kawamura, T. Yokoo, T. Nakatani, R. Maruyama, K. Soyama, K. Shibata, K. Suzuya, S. Sato, K. Aizawa, M. Arai, S. Wakimoto, M. Ishikado, S.-i. Shamoto, M. Fujita, H. Hiraka, K. Ohoyama, K. Yamada, and C.-H. Lee, “The Fermi chopper spectrometer 4SEASONS at J-PARC,” *J. Phys. Soc. Jpn.* **80**, SB025 (2011).
- [43] Y. Inamura, T. Nakatani, J. Suzuki, and T. Otomo, “Development status of software “Utsusemi” for chopper spectrometers at MLF, J-PARC,” *J. Phys. Soc. Jpn.* **82**, SA031 (2013).
- [44] R. D. Shannon, “Revised effective ionic radii and systematic studies of interatomic distances in halides and chalcogenides,” *Acta Crystallogr. A* **32**, 751–767 (1976).
- [45] R.-D. Hoffmann and Rainer Pöttgen, “AlB₂-related intermetallic compounds—a comprehensive view based on group-subgroup relations,” *Z. Kristallogr. Cryst. Mater.* **216**, 127 (2001).
- [46] Y.-L. Wang, “Crystal-field effects of paramagnetic Curie temperature,” *Phys. Lett. A* **35**, 383–384 (1971).
- [47] P. Boutron, “Exact calculation of the paramagnetic susceptibility of a single crystal with arbitrary crystal field and exchange interactions,” *Phys. Rev. B* **7**, 3226 (1973).
- [48] N. Van Hieu, T. Takeuchi, H. Shishido, C. Tonohiro, T. Yamada, H. Nakashima, K. Sugiyama, R. Settai, T. D. Matsuda, Y. Haga, *et al.*, “Magnetic properties and crystalline electric field scheme in $RRhIn_5$ (R : Rare earth),” *J. Phys. Soc. Jpn.* **76**, 064702 (2007).
- [49] Y. Li, S. Bachus, H. Deng, W. Schmidt, H. Thoma, V. Hutnanu, Y. Tokiwa, A. A. Tsirlin, and P. Gegenwart, “Partial up-up-down order with the continuously distributed order parameter in the triangular antiferromagnet TmMgGaO₄,” *Phys. Rev. X* **10**, 011007 (2020).
- [50] Y. Shen, C. Liu, Y. Qin, S. Shen, Y.-D. Li, R. Bewley, A. Schneidewind, G. Chen, and J. Zhao, “Intertwined dipolar and multipolar order in the triangular-lattice magnet TmMgGaO₄,” *Nat. Commun.* **10**, 1–7 (2019).
- [51] M. Doerr, M. Rotter, and A. Lindbaum, “Magnetostriction in rare-earth based antiferromagnets,” *Adv. Phys.* **54**, 1 (2005).
- [52] B. Grover, “Dynamical properties of induced-moment systems,” *Phys. Rev.* **140**, A1944 (1965).
- [53] E. A. Goremychkin, R. Osborn, B. D. Rainford, R. T. Macaluso, D. T. Adroja, and M. Koza, “Spin-glass order induced by dynamic frustration,” *Nat. Phys.* **4**, 766–770 (2008).
- [54] K. Andres, E. Bucher, S. Darack, and J. P. Maita, “Induced-moment ferromagnetism in Pr₃Tl,” *Phys. Rev. B* **6**, 2716 (1972).
- [55] H. Kitazawa, A. Dönni, L. Keller, J. Tang, F. Fauth, and G. Kido, “Magnetic structures of the rare-earth platinum aluminides $RPtAl$ ($R = Ce, Pr, Nd$),” *J. Solid State Chem.* **140**, 233–241 (1998).
- [56] V. K. Anand, D. T. Adroja, A. Bhattacharyya, A. D. Hillier, J. W. Taylor, and A. M. Strydom, “Investigations of the singlet ground state system: PrIrSi₃,” *J. Phys.: Condens. Matter* **26**, 306001 (2014).
- [57] P. G. De Gennes, “Indirect interactions between 4f shells in rare earth metals,” *J. Phys. Radium* **23**, 510 (1962).
- [58] Z.-S. Liu and S.-L. Guo, “Transition temperatures of rare-earth compounds studied with perturbation theory,” *Phys. Lett. A* **314**, 491–497 (2003).
- [59] D. R. Noakes and G. K. Shenoy, “The effect of a crystalline electric field on the magnetic transition temperatures of rare-earth rhodium borides,” *Phys. Lett. A* **91**, 35–36 (1982).
- [60] N. H. Luong, J. J. M. Franse, and N. H. Hai, “Effect of the crystalline electric field on the Néel temperatures of RCu_2 compounds,” *J. Magn. Magn. Mater.* **224**, 30–32 (2001).
- [61] M. E. Lines, “Sensitivity of Curie temperature to single-ion anisotropy,” *Phys. Rev. B* **12**, 3766 (1975).
- [62] D. Hickox-Young, D. Puggioni, and J. M. Rondinelli, “Polar metals taxonomy for materials classification and discovery,” arXiv preprint arXiv:2210.05110 (2022).
- [63] S. Bhowal and N. A. Spaldin, “Polar metals: principles and prospects,” arXiv preprint arXiv:2210.02993 (2022).